Title	Grating couplers in silicon-on-insulator: The role of photonic guided resonances on lineshape and bandwidth
Authors	Passoni, M.;Gerace, Dario;Carroll, Lee;Andreani, L. C.
Publication date	2017-01-27
Original Citation	Passoni, M., Gerace, D., Carroll, L. and Andreani, L. C. (2017) 'Grating couplers in silicon-on-insulator: The role of photonic guided resonances on lineshape and bandwidth', Applied Physics Letters, 110(4), pp. 041107. doi:10.1063/1.4974992
Type of publication	Article (peer-reviewed)
Link to publisher's version	10.1063/1.4974992
Rights	© 2017, AIP Publishing. This article may be downloaded for personal use only. Any other use requires prior permission of the author and AIP Publishing. The following article appeared in Appl. Phys. Lett. 110, 041107 (2017) and may be found at http://aip.scitation.org/doi/abs/10.1063/1.4974992
Download date	2024-04-18 16:38:51
Item downloaded from	https://hdl.handle.net/10468/3549

Grating couplers in silicon-on-insulator: The role of photonic guided resonances on lineshape and bandwidth

M. Passoni, D. Gerace, L. Carroll, and L. C. Andreani

Articles you may be interested in

Grating couplers in silicon-on-insulator: The role of photonic guided resonances on lineshape and bandwidth

M. Passoni,[1] D. Gerace,[1] L. Carroll,[2] and L. C. Andreani[1]

[1]*Department of Physics and CNISM, University of Pavia, 27100 Pavia, Italy*
[2]*Tyndall National Institute, Cork, Ireland*

Most grating couplers for silicon photonics are designed to match the approximately 10 μm mode-field diameter (MFD) of single-mode telecom fibres. In this letter, we analyse grating-coupler designs in the Silicon-on-Insulator (SOI) platform in a wide range of MFDs (4–100 μm) and related footprints, to give a physical understanding of the trends in efficiency and lineshape of the corresponding coupling spectra. We show that large-footprint grating couplers have an intrinsic Lorentzian lineshape that is determined by the quasi-guided photonic modes (or guided resonances) of the corresponding photonic crystal slab, while small-footprint grating couplers have a Gaussian lineshape resulting from the k-space broadening of the incident mode. The crossover between the two regimes is characterized by Voigt lineshapes. Multi-objective particle-swarm optimisation of selected small-footprint apodized grating-couplers is then used to locate the "Pareto fronts;" along which the highest coupling efficiency is achieved for a given bandwidth. This approach identifies several high-efficiency 220 nm SOI grating coupler designs with 1 dB bandwidths exceeding 100 nm. Such grating couplers are ideally suited for broadband photonic applications, such as wavelength-division multiplexing and environmental sensing, and are compatible with commercially available ultra-high numerical aperture fibres. *Published by AIP Publishing.*
[http://dx.doi.org/10.1063/1.4974992]

Silicon photonics can be used to fabricate highly integrated devices for Information and Communication Technology (ICT), medical, and sensing applications.[1–6] A large body of research and product development in silicon photonics has been carried-out on the 220 nm silicon-on-insulator (SOI) platform, where the high index contrast between layers, and the low absorption in the O- and C- telecom bands, allow for small and potentially cost-effective photonic integrated circuits (PICs) to be directly interfaced to long-distance communication channels. The same platform is also employed to realize many of the silicon-based photonic crystal (PhC) slabs.[7,8] These are waveguide embedded structures that are able to control the propagation and confinement of electromagnetic signals either by exploiting guided resonances (lossy, lying above the light line and coupled to electromagnetic waves in the far-field) or truly guided modes (ideally lossless, lying below the light line and evanescent in the low-index claddings).[9–13]

Currently, a key challenge for realising practical PIC devices is the development of fibre-to-chip coupling that offers low optical insertion losses, and is compatible with the photonic packaging technology for scaling up to volume manufacture. Grating-couplers[14–17] are one possible solution, because they offer relatively relaxed alignment tolerances, do not require precision dicing or polishing of the PIC, and allow for wafer-scale performance testing. The two main figures of merit for grating couplers are (i) the coupling efficiency (CE), which defines the fraction of light transferred from the incident fibre-mode into the SOI waveguides, and (ii) the bandwidth of the coupling spectrum, commonly defined as the spectral broadening at 1 dB from the maximum CE, which represents the useful spectral window. Notice that a uniform grating coupler is nothing else than a 1D or 2D photonic crystal (PhC) slab with a partial etching of the silicon core layer.

CE values of more than 80% (i.e., insertion losses better than 1 dB) can be achieved in state-of-the art 1D SOI grating-couplers that take advantage of nonuniform[18–21] or sub-wavelength[22–24] patterning, poly-Si layers added during lithography,[25] and the replacement of the Si-substrate with metallic bottom-reflectors.[26] In parallel, the optimisation of 2D grating coupler designs has largely eliminated the polarisation sensitivity of 1D structures, allowing for an efficient fibre-to-chip coupling regardless of the polarisation-state of the incident mode.[16,17,27–31]

The bandwidth of SOI grating-couplers tends to be limited to 30–40 nm, which is adequate for single-wavelength photonics, but limits the suitability for broadband applications, such as wavelength division multiplexing for high bandwidth ICT devices, or environmental and security sensors that probe multiple gas-lines. Specific designs that offer increased bandwidth have been demonstrated, usually featuring complex structures such as dual-level gratings,[32–34] sub-wavelength patterning[24,35,36] or use of smaller fibers.[33,34] Theoretical models for the trends of the bandwidth have been developed in the case of uniform gratings.[37] Still, general studies of the relationship between the CE and bandwidth of grating couplers have not been reported so far.

Grating couplers are most often considered in a range of footprints that match the mode-field diameter (MFD) of standard single-mode fibers (10.4 μm). In this work we study grating couplers in a wide range of MFDs (4–100 μm), also implying a variable footprint. We focus on 1D gratings with 220 nm thickness of the silicon core layer operating at the telecom wavelength $\lambda = 1.55$ μm in transverse electric (TE)
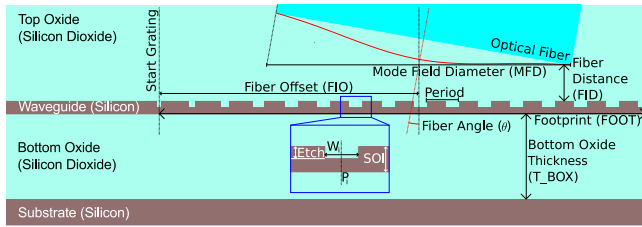
FIG. 1. Schematic illustration of the structure of the one-dimensional grating couplers studied in this work, where all the relevant parameters involved are explicitly defined. Refractive indices are: $n(\text{Si}) = 3.47$ and $n(\text{oxide}) = 1.44$.

polarization (the electric field of the incident beam is parallel to the waveguide plane, perpendicular to the cross-section of Fig. 1) and with a fiber angle fixed at $10°$. Our goal is two-fold: First, we analyze the origin of the coupling between an optical fiber mode and a silicon waveguide in terms of the physics of a PhC slab. To this purpose, we study the line-shape and bandwidth of uniform couplers in terms of the radiative losses of quasi-guided modes. Second, for selected values of the MFD, we simultaneously optimize the CE and the bandwidth of apodized grating couplers. We adopt a multi-objective particle-swarm optimization (MO-PSO) algorithm in order to identify improved high-bandwidth, high-CE designs. The results of this work clarify the different physical regimes of grating coupler operation, and show that tuning the MFD is a promising route to realize large-bandwidth devices.

The main parameters of our structures are shown in Fig. 1. For uniform gratings, the lattice is defined by the period and by a duty cycle DC (i.e., the constant value of the groove width over the period), while for non-uniform gratings, each groove is characterized by its own position and width. Each structure is numerically analysed by using Finite-Difference Time-Domain (FDTD) simulations.[38] The light coming from the fiber is simulated by a Gaussian beam, whose MFD is the diameter at which the electric field amplitude is reduced by a factor of $1/e$ with respect to the peak value. The grating foot-print (FOOT in Fig. 1) can be more extended than the MFD, and the fiber mode is separated from the silicon waveguide by a fiber offset (FIO in Fig. 1). The most significant parameter is the MFD: we have verified that the performance of the grating coupler is nearly independent of the footprint once it is large enough to accommodate the whole fiber mode. In this work, we study the grating properties as a function of MFD, properly optimizing the fiber offset FIO and taking FOOT to be slightly

larger than MFD. Additional details are given in the supplementary material (SM), Secs. I and II.

The behavior of a grating coupler can be understood by studying the physics of photonic crystals embedded in planar waveguides, usually known as PhC slabs.[7] Adding a periodic pattern in a planar waveguide induces a folding of slab guided modes into the first Brillouin zone. The bands that are folded above the cladding light line become quasi-guided with a finite linewidth over the continuum background represented by radiative modes.[10–12] The partially etched grating coupler represents a weak photonic perturbation on a planar waveguide, but the same concept of band folding holds. In fact, we can understand the coupling of light from free space into or from the waveguide as arising from the resonance condition between far-field radiation—whose dispersion lies above the cladding light cone—and a quasi-guided mode, as schematically represented in Fig. 2(a). The PhC slab theory strictly holds for infinite systems, while in a finite system, the incident beam has a broadening in k-space. This leads to a frequency broadening of the resonance condition, as illustrated in Fig. 2(b) and further discussed below.

We have performed a systematic study of CE and bandwidth for uniform 1D gratings as a function of the MFD, for different values of the etching depth. Throughout this analysis, we fixed the thickness of bottom oxide to $2\,\mu$m, which was previously shown to be an optimal value for 1D grating couplers.[21] In general, the CE has a periodic dependence on the BOX thickness, as it is affected by constructive/destructive interference between the incoming and the reflected wave at the bottom interface. We also fixed the ratio between the fiber offset and the MFD to 0.470, while the period of each grating coupler was tuned to lock the maximum CE at $\lambda = 1.55\,\mu$m.

The resulting CE and bandwidth as a function of MFD are shown in Fig. 3, where the bandwidth is evaluated as the full width at half maximum (FWHM) of the corresponding coupling resonance. The behavior of the CE shows an optimal MFD, depending on the etching depth considered. This can be understood by considering that light in a patterned waveguide can only propagate for a finite distance due to the out-of-plane diffraction.[9–13] When the MFD exceeds such a distance, only the light that is absorbed near the edge of the grating can propagate until the unpatterned waveguide, leading to a decrease of coupling efficiency. Simultaneously, the bandwidth shows a decreasing trend as a function of the MFD, tending to saturate at a constant value.
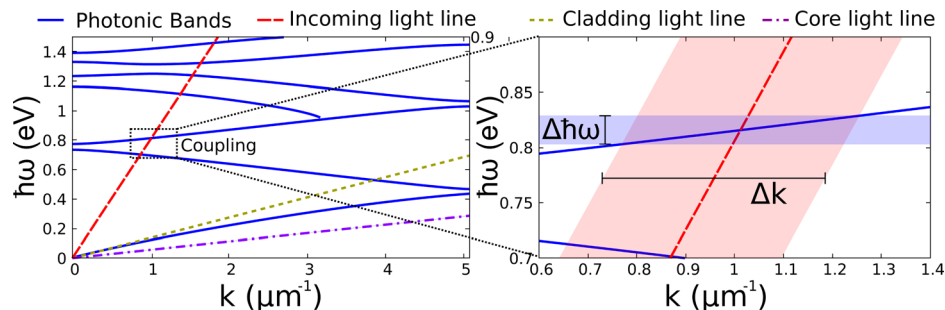

FIG. 2. (a) Schematic illustration of band folding induced by a periodic pattern onto a planar waveguide, and (b) coupling of an incident beam with k-space broadening through resonance with a quasi-guided mode, resulting in a frequency broadening. Parameters: etch depth 80 nm, period 619 nm, DC = 25%. The incoming light line represents the dispersion of a plane wave coming from the top cladding at an incident angle of $10°$, namely, $\omega = ck/(n_{clad} \sin 10°)$.
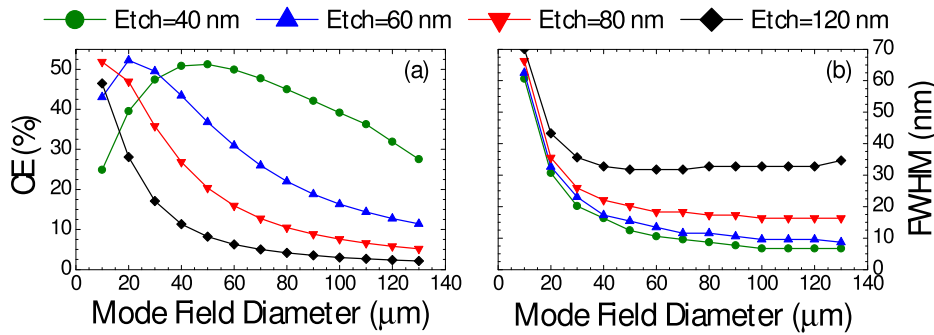
FIG. 3. Numerically calculated (a) coupling efficiency and (b) bandwidth (FWHM) as a function of MFD, for different etching depths. Fixed parameters: DC = 25%, T_BOX = 2 μm. The period is tuned for coupling at $\lambda = 1.55\,\mu m$.

We claim that the bandwidth behavior can be understood in terms of two contributions: The first one is due to the finite dimensions of the excitation spot, while the second one is related to the intrinsic loss rate of the quasi-guided mode involved in the coupling. For the first mechanism, an excitation with a Gaussian beam leads to a Gaussian spread in wavevector σ_k that can be derived from the Fourier transform of the mode profile in real space. This is at the origin of a spread in energy σ_ω, which arises from the coupling between the k-broadened incident mode and the guided modes (see Fig. 2(b)). The relation between σ_ω and the MFD can be written as

$$\frac{\sigma_\omega}{\omega} = \frac{2\lambda}{\pi n_{\text{eff}} \text{MFD}}, \qquad (1)$$

where n_{eff} is an effective waveguide index. The second contribution arises from the intrinsic radiative linewidth of quasi-guided PhC modes, leading to a homogeneous broadening with a Lorentzian lineshape, and it is expected to be constant as soon as the MFD is large enough.

Our hypothesis is confirmed by the simulated spectra, shown in Fig. 4 for a few selected cases. The lineshape is Gaussian in the region of small MFD, well before saturation of the bandwidth in Fig. 3(b), and it becomes Lorentzian for large MFD. We notice that for the intermediate case, the lineshape is very well fitted with a Voigt profile, which is a convolution between Gaussian and Lorentzian lineshapes, as expected when both contributions are relevant. Such behaviour as a function of footprint has been found for all the analyzed structures.

To further test our interpretation, we have compared the results of 2D-FDTD simulations to a Rigorous Coupled Wave Analysis (RCWA) of the corresponding infinite structures.[39,40] We briefly remind that RCWA allows to calculate the transmission and reflection spectra of arbitrarily layered PhC slabs with 1D or 2D patterns. To separate the Gaussian and Lorentzian contributions to the bandwidth, we have fitted each spectrum from FDTD simulations with a Voigt profile. This yields the broadening parameters σ and γ, namely, the standard deviation of the Gaussian and the half-width at

half maximum of the Lorentzian lineshapes involved in the convolution, respectively. From the RCWA calculation, reflection spectra of the corresponding PhC slab give Fano-type resonances that arise from coupling of the quasi-guided modes with the continuum background of radiative slab modes.[11,41] The Fano fit allows to extract the real and imaginary parts of the resonance frequency of quasi-guided modes. The Gaussian contribution to the bandwidth can be obtained knowing the frequency of the coupling resonance and applying momentum conservation. An example of such a comparison is presented in Fig. 5, where we notice an overall good agreement between the two approaches. The only discrepancy arises for the Lorentzian contribution at small MFD. Such a discrepancy vanishes at larger MFD, and it can be attributed to the few lattice periods corresponding to a small MFD, where the very concept of a photonic crystal becomes less relevant.

Summarizing the present analysis, we confirm that the bandwidth of uniform grating couplers follows from two contributions identified as a finite-size one (k-space broadening of the Gaussian beam) and an infinite-size term arising from the intrinsic radiative broadening of quasi-guided modes. The bandwidth increases on reducing the MFD, thus smaller MFD structures might be interesting for applications requiring a compromise between large CE and bandwidth.

The second goal of the present work is to find a route to increase the operational bandwidth of SOI grating couplers without compromising the CE. Hence, we have to go beyond uniform gratings to simultaneously optimize the CE and bandwidth, by applying the concept of *apodization* (i.e., individual modification of each grating groove). Several studies have already been performed in this direction, often adopting sophisticated optimization procedures.[34,42–44]

Here we employ an optimization algorithm known as Particle Swarm Optimization (PSO),[45] owing to its relatively easy implementation and its good performance in electromagnetic problems.[42,46,47] The use of such type of algorithm for simultaneous optimization of bandwidth and CE of grating couplers has already been reported in the literature.[48–50] In the present work, we implement a Multi-Objective version of PSO (MO-PSO) based on the concept of "Pareto front."[51]
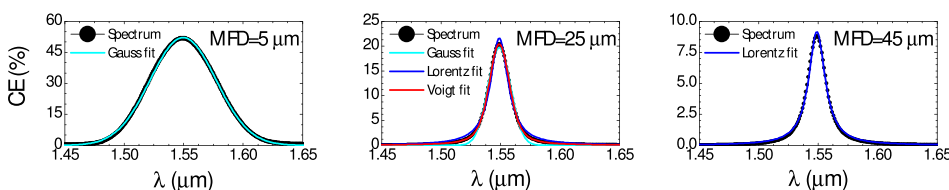

FIG. 4. Simulated coupling spectra for structures with 80 nm etching depth (all other parameters as in Fig. 3), considering different values of MFD. The spectra are well fitted by Gaussian (a), Voigt (b), and Lorentzian lineshapes (c), respectively.
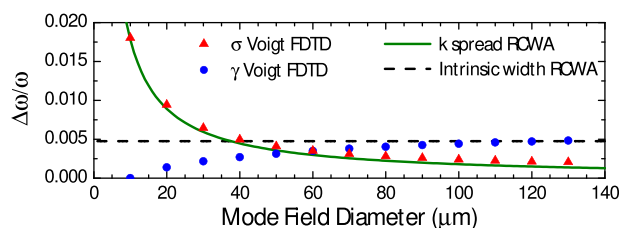
FIG. 5. Comparison of Gaussian (σ) and Lorentzian (γ) contributions to the bandwidth as calculated by 2D-FDTD (points) and RCWA (lines), respectively. Fixed parameters are as in Figs. 3 and 4 ($n_{\mathrm{eff}} = 2.77$).

Here, we are allowed to optimize a set of fitness functions, each expressing a single objective, which in our case correspond to the CE and bandwidth. The Pareto improvement of a structure is defined as a modification that improves at least one fitness function without decreasing any other. Hence, a Pareto front can be defined as the ensemble of all the structures that cannot be further Pareto improved. Thus, the knowledge of the Pareto front for the given problem gives an exhaustive set of optimal structures. The optimization algorithm works iteratively: The temporary Pareto front is stored at each step, and it should converge to the real Pareto front with a sufficient number of iterations.

The MO-PSO is combined with 2D-FDTD simulations to simultaneously optimize the CE and bandwidth, the latter being defined in the following at -1 dB from the maximum CE. We vary the width and position of each grating element for four different MFDs, namely, the standard value 10.4 μm, and three smaller values given by 8, 6 and 4 μm. As a starting point of the optimization procedure, we use the knowledge of the linearly chirped structure with the best CE for each MFD. The latter can be found by a dedicated Single-Objective PSO. Each optimization was run with 20 agents for 1000 iterations, exploring a total of 2×10^4 configurations. In the case of 10.4 μm MFD, a further optimization run was undertaken in conjunction with the tolerance analysis, see supplementary material (SM) for details.

The results are shown in Fig. 6 for the four Pareto fronts obtained considering different MFDs. It clearly emerges that a precise trade-off exists between the CE and bandwidth, once the MFD has been fixed. On this front, no improvement can be made in one of the two quantities without compromising the other. Moreover, it is clearly evidenced that decreasing the MFD generally increases the bandwidth, even if it comes at the expense of a slight reduction of the maximum
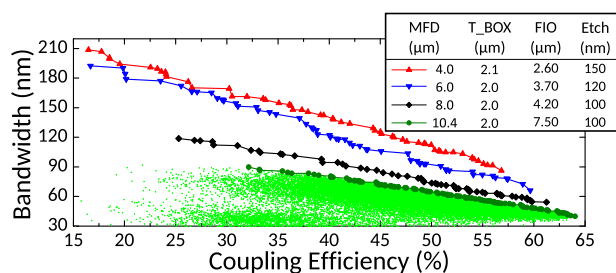

FIG. 6. Pareto fronts obtained for different MFDs. For MFD = 10.4 μm, the CE and 1 dB bandwidth are plotted also for all the structures analyzed through the optimization (light green), to help the reader visualizing the Pareto front as a true front of a much larger set of data. The table reports the parameters common to all the structures of each Pareto front.

achievable CE. As an illustrative example, going from 10.4 μm to 4 μm, the bandwidth is doubled while only 7% is lost in CE. The target of 100 nm bandwidth (suitable for wavelength-division multiplexing transmission with 4 channels) can be achieved with a 47% CE, by simply using a 6 μm MFD, further improved to 53% if a 4 μm MFD is used. Such values can be obtained using lensed fibers (as done, e.g., in Ref. 34) or tapered fibers.

The Pareto fronts of Fig. 6 turn out to follow a nearly linear behaviour for all values of the MFD. They result from a complex multi-parameter optimization and cannot be expressed by a simple model. Still, the analysis of the structures on the Pareto fronts (see supplementary material, Sec. VI for details) yields some insight into the outcome of the optimization procedure. For the points with highest CE in a Pareto front, the apodized structure is characterized by a transition region with a smooth increase of the groove width from the edge of the grating towards the central part: this provides impedance matching between the guided mode of the grating and that of the silicon waveguide. Moving up on the Pareto front, the transition region and the whole grating become progressively more disordered: the increase of disorder results in an increase in bandwidth, thanks to the wider spectrum of Fourier components, but reduces the CE as both resonance coupling and impedance matching are less effective.

We have presented a theoretical analysis of bandwidth and coupling efficiency for one-dimensional grating couplers in the 220 nm SOI platform. For uniform gratings, we find that the bandwidth monotonically decreases when increasing the MFD, and it is mainly composed of two contributions. The first one, coming from the finite size and the resulting k-space broadening of the incoming beam, dominates at smaller MFD, while the second one, related to the intrinsic linewidth of the photonic quasi-guided mode, dominates at larger MFD. This is also confirmed by analysing the coupling lineshape, which shows a Gaussian behavior for small MFD, and a Lorentzian behavior when the photonic crystal regime (the limit of infinitely extended lattice) sets in. Using an MFD smaller than the standard value of 10.4 μm, we have shown that it is possible to sensitively increase the grating couplers bandwidth. In particular, a 4 μm MFD allows increasing the bandwidth from about 40 nm to 100 nm, while the coupling efficiency is reduced only from 65% to 53%. Depending on the use of suitable fibers with reduced spot size, these results suggest a strategy for the realization of grating couplers supporting several channels for optical communication in a standard SOI platform. Further improvements are expected by the use of SOI with thicker (e.g., $\geq$300 nm) silicon layers.

See supplementary material (SM) for details on the numerical procedures, for a complete data of the structures on the Pareto fronts, and for a tolerance analysis.

[1] R. Soref, IEEE J. Sel. Top. Quantum Electron. **12**, 1678 (2006).
[2] B. Charbonnier, S. Menezo, P. O'Brien, A. Lebreton, J. M. Fedeli, and B. B. Bakir, IEEE/OSA J. Opt. Commun. Networking **4**, A29 (2012).

[3]M. Streshinsky, R. Ding, Y. Liu, A. Novack, C. Galland, A.-J. Lim, P. G.-Q. Lo, T. Baehr-Jones, and M. Hochberg, Opt. Photonics News **24**, 32 (2013).

[4]P. Dong, Y. Chen, G. Duan, and D. T. Neilson, Nanophotonics **3**, 215 (2014).

[5]D.-X. Xu, J. H. Schmid, G. T. Reed, G. Z. Mashanovich, D. J. Thomson, M. Nedeljkovic, X. Chen, D. Van Thourhout, S. Keyvaninia, and S. K. Selvaraja, IEEE J. Sel. Top. Quantum Electron. **20**, 189 (2014).

[6]C. Sun, M. T. Wade, Y. Lee, J. S. Orcutt, L. Alloatti, M. S. Georgas, A. S. Waterman, J. M. Shainline, R. R. Avizienis, and S. E. A. Lin, Nature **528**, 534 (2015).

[7]J. D. Joannopoulos, S. G. Johnson, J. N. Winn, and R. D. Meade, *Photonic Crystals: Molding the Flow of Light*, 2nd ed. (Princeton University Press, 2008).

[8]K. Sakoda, *Optical Properties of Photonic Crystals* (Springer Science & Business Media, 2004).

[9]S. G. Johnson, S. Fan, P. R. Villeneuve, J. D. Joannopoulos, and L. A. Kolodziejski, Phys. Rev. B **60**, 5751 (1999).

[10]T. Ochiai and K. Sakoda, Phys. Rev. B **63**, 125107 (2001).

[11]S. Fan and J. D. Joannopoulos, Phys. Rev. B **65**, 235112 (2002).

[12]D. Gerace and L. C. Andreani, Phys. Rev. E **69**, 056603 (2004).

[13]L. C. Andreani and D. Gerace, Phys. Rev. B **73**, 235114 (2006).

[14]D. Taillaert, P. Bienstman, and R. Baets, Opt. Lett. **29**, 2749 (2004).

[15]W. Bogaerts, D. Taillaert, P. Dumon, D. Van Thourhout, R. Baets, and E. Pluk, Opt. Express **15**, 1567 (2007).

[16]G. Roelkens, D. Vermeulen, F. Van Laere, S. Selvaraja, S. Scheerlinck, D. Taillaert, W. Bogaerts, P. Dumon, D. Van Thourhout, and R. Baets, J. Nanosci. Nanotechnol. **10**, 1551 (2010).

[17]A. Mekis, S. Gloeckner, G. Masini, A. Narasimha, T. Pinguet, S. Sahni, and P. D. Dobbelaere, IEEE J. Sel. Top. Quantum Electron. **17**, 597 (2011).

[18]X. Chen, C. Li, C. K. Fung, S. M. Lo, and H. K. Tsang, IEEE Photonics Technol. Lett. **22**, 1156 (2010).

[19]M. Antelius, K. B. Gylfason, and H. Sohlström, Opt. Express **19**, 3592 (2011).

[20]Y. Ding, C. Peucheret, H. Ou, and K. Yvind, Opt. Lett. **39**, 5348 (2014).

[21]A. Bozzola, L. Carroll, D. Gerace, I. Cristiani, and L. C. Andreani, Opt. Express **23**, 16289 (2015).

[22]R. Halir, P. Cheben, S. Janz, D.-X. Xu, Í. Molina-Fernández, and J. G. Wangüemert-Pérez, Opt. Lett. **34**, 1408 (2009).

[23]D. Benedikovic, P. Cheben, J. H. Schmid, D.-X. Xu, J. Lapointe, S. Wang, R. Halir, A. Ortega-Moñux, S. Janz, and M. Dado, Laser Photonics Rev. **8**, L93 (2014).

[24]D. Benedikovic, P. Cheben, J. H. Schmid, D. Xu, B. Lamontagne, S. Wang, J. Lapointe, R. Halir, A. Ortega-Moñux, S. Janz, and M. Dado, Opt. Express **23**, 22628 (2015).

[25]D. Vermeulen, S. Selvaraja, P. Verheyen, G. Lepage, W. Bogaerts, P. Absil, D. Van Thourhout, and G. Roelkens, Opt. Express **18**, 18278 (2010).

[26]W. S. Zaoui, A. Kunze, W. Vogel, M. Berroth, J. Butschke, F. Letzkus, and J. Burghartz, Opt. Express **22**, 1277 (2014).

[27]L. Liu, M. Pu, K. Yvind, and J. M. Hvam, Appl. Phys. Lett. **96**, 051126 (2010).

[28]X. Chen and H. K. Tsang, Opt. Lett. **36**, 796 (2011).

[29]L. Carroll, D. Gerace, I. Cristiani, S. Menezo, and L. C. Andreani, Opt. Express **21**, 21556 (2013).

[30]L. Carroll, D. Gerace, I. Cristiani, and L. C. Andreani, Opt. Express **22**, 14769 (2014).

[31]J. Zou, Y. Yu, and X. Zhang, Opt. Express **23**, 32490 (2015).

[32]W. D. Sacher, Y. Huang, L. Ding, B. J. Taylor, H. Jayatilleka, G. Lo, and J. K. Poon, Opt. Express **22**, 10938 (2014).

[33]M. T. Wade, F. Pavanello, R. Kumar, C. M. Gentry, A. Atabaki, R. Ram, V. Stojanović, and M. A. Popović, in *IEEE Optical Interconnects Conference (OI)* (IEEE, 2015), pp. 46–47.

[34]J. Notaros, F. Pavanello, M. T. Wade, C. Gentry, A. Atabaki, L. Alloatti, R. J. Ram, and M. Popovic, in *Optical Fiber Communication Conference* (Optical Society of America, 2016), p. M2I.5.

[35]X. Chen, K. Xu, Z. Cheng, C. K. Fung, and H. K. Tsang, Opt. Lett. **37**, 3483 (2012).

[36]A. Sánchez-Postigo, J. G. Wangüemert-Pérez, J. M. Luque-González, Í. Molina-Fernández, P. Cheben, C. A. Alonso-Ramos, R. Halir, J. H. Schmid, and A. Ortega-Moñux, Opt. Lett. **41**, 3013 (2016).

[37]Z. Xiao, T. Liow, J. Zhang, P. Shum, and F. Luan, Opt. Express **21**, 5688 (2013).

[38]See https://www.lumerical.com/tcad-products/fdtd/ for FDTD software from Lumerical Solutions, Inc.

[39]D. M. Whittaker and I. S. Culshaw, Phys. Rev. B **60**, 2610 (1999).

[40]M. Liscidini, D. Gerace, L. C. Andreani, and J. E. Sipe, Phys. Rev. B **77**, 035324 (2008).

[41]M. Galli, D. Bajoni, M. Belotti, F. Paleari, M. Patrini, G. Guizzetti, D. Gerace, M. Agio, L. C. Andreani, D. Peyrade, and Y. Chen, IEEE J. Sel. Areas Commun. **23**, 1402 (2005).

[42]B. Wohlfeil, L. Zimmermann, and K. Petermann, Opt. Lett. **39**, 3201 (2014).

[43]A. Piggott, J. Lu, T. Babinec, K. Lagoudakis, J. Petykiewicz, and J. Vučković, Sci. Rep. **4**, 7210 (2014).

[44]J. Notaros and M. A. Popović, Opt. Lett. **40**, 1053 (2015).

[45]R. C. Eberhart and J. Kennedy, in *Proceedings of the Sixth International Symposium on Micro Machine and Human Science* (IEEE, 1995), Vol. 1, pp. 39–43.

[46]J. Robinson and Y. Rahmat-Samii, IEEE Trans. Antennas Propag. **52**, 397 (2004).

[47]N. Jin and Y. Rahmat-Samii, IEEE Trans. Antennas Propag. **55**, 556 (2007).

[48]S. Selvaraja, D. Vermeulen, M. Schaekers, E. Sleeckx, W. Bogaerts, G. Roelkens, P. Dumon, D. Van Thourhout, and R. Baets, in *Conference on Lasers and Electro-Optics/International Quantum Electronics Conference, OSA Technical Digest* (IEEE, 2009), p. CTuC6.

[49]Q. Zhong, V. Veerasubramanian, Y. Wang, W. Shi, D. Patel, S. Ghosh, A. Samani, L. Chrostowski, R. Bojko, and D. V. Plant, Opt. Express **22**, 18224 (2014).

[50]Y. Wang, H. Yun, Z. Lu, R. Bojko, W. Shi, X. Wang, J. Flueckiger, F. Zhang, M. Caverley, N. A. Jaeger, and L. Chrostowski, IEEE Photonics J. **7**, 2400110 (2015).

[51]P. K. Tripathi, S. Bandyopadhyay, and S. K. Pal, in *IEEE Congress on Evolutionary Computation* (IEEE, 2007), pp. 2281–2288.